(Received 1 October 2024, Accepted 29 October 2024, Scheduled 8 November 2024)

Stochastic Investigation of the Input Impedance of Vertical, Horizontal, and Arbitrarily Oriented Elementary Dipoles in Proximity to a Perfectly Conducting or Dielectric Ground

Aikaterini Mangou[1], George P. Veropoulos[2, 3], Constantinos Vlachos[4], and Panagiotis J. Papakanellos[5, *]

[1] *Hellenic Air Force, Greece*
[2] *Hellenic Navy's Petty Officers' Academy, Skaramagkas, GR 12400 Athens, Greece*
[3] *Hellenic Naval Academy, Hadjikyriakou Avenue, GR 18539 Piraeus, Greece*
[4] *Hellenic Navy's Naval Weapons Directorate, Salamis Naval Base, GR 18900 Salamis, Greece*
[5] *Hellenic Air Force Academy, GR 13671 (1010) Dekelia, Athens, Greece*

ABSTRACT: Antennas operating in the close vicinity of obstacles or scatterers behave much different from isolated antennas radiating in free space. To assess such interactions in which a large number of parameters are involved (pertaining to the geometry, possible movement effects, and materials), stochastic models are often conceived and adopted so as to cope with innate uncertainties and to overcome the need for time-consuming parametric investigations. In this paper, an analytical stochastic approach is presented for the archetypical problems of the vertical, horizontal, and arbitrarily oriented dipole above a semi-infinite ground (either perfectly conducting or dielectric). The analysis focuses on how the input impedance of the dipole is affected by the existence of the ground plane when the distance or the angle between them varies in accordance with some certain probability distributions. Approximate closed-form expressions are obtained for the probability distributions of the input resistance and reactance respectively, which can directly yield the respective moments and variances (and potentially other quantitative measures) and are useful for characterizing the probabilistic behavior of the dipole and its interaction with the ground. Representative numerical results are presented aiming at the validation of the proposed model and the investigation of the probabilistic behavior of the impedance change. Finally, a few concluding remarks are outlined, and possible extensions to real-world problems are discussed.

1. INTRODUCTION

Antennas and antenna arrays are usually strongly affected, even disrupted, when they operate in proximity to objects acting as scatterers or absorbers of electromagnetic waves. Some exceptions to this rule are very directional antennas (e.g., radar pencil-beam antennas) and smart arrays with strong adaptation/mitigation capabilities. Apart from such exceptions, the interactions between antennas and obstacles/scatterers in their near-field region become more pronounced, often causing severe deterioration of the antenna's performance, when the distance between them or/and their relevant orientation changes with time. Such interactions take place in numerous practical applications, including the coupling between handset and user head/arm/body in personal/mobile communications, as well as temporal/spatial variations and fading effects due to bouncing of an antenna (e.g., straight/helical wire antennas) on the roof of a moving platform (e.g., car, vessel, aircraft, spacecraft, rover moving on a rough terrain). The practical relevance of the results of this study to such more complex scenarios will be established below.

As an outcome of the strong coupling between an antenna and an object in its close vicinity, the antenna currents are altered significantly, a fact that is further manifested in the deviation of the transmitting/receiving characteristics from the ones pertaining to the antenna's free-space behavior. These regard both near-field and far-field quantities, including input impedance, radiation/reception patterns, the axial ratio of the radiating field, as well as the efficiency of the antenna [1–5].

Despite the importance of the aforementioned issues, antennas in the presence of (relatively) moving objects are rarely assessed analytically, mainly due to modeling difficulties and to lack of confidence in establishing an adequate stochastic model for the description of the varying geometry, let alone the complexity in the description of the coupling itself, especially for scatterers/obstacles of non-canonical geometry. Even canonical cases, such as elementary dipoles close to spheres [6], are too difficult to handle analytically and are perhaps too computationally intensive for a purely numerical assessment. On the other hand, stochastic models and numerical approaches have been proposed and used in many ways, as they seem to overcome many of the aforementioned difficulties in an effective and often comprehensive manner, e.g., see [7–20] for studies exploiting stochastic tools for purposes rather different from those of this study. The study of this paper differs notably from other works, as long as it regards a toy problem and is based solely on classic antenna theory in order to obtain closed-

* Corresponding author: Panagiotis J. Papakanellos (panagiotis.papakanellos@hafa.haf.gr).

form results by applying probability theory. Nevertheless, none of [7–20] focuses on the antenna itself from this perspective, and the cases discussed therein are much more demanding and not easily tractable using analytical tools.

In this paper, a simple and tangible analytical model is presented for the stochastic assessment of electrically short dipoles carrying constant currents (i.e., Hertzian dipoles) radiating close to either a perfect ground (i.e., an infinite in extent and perfectly conducting screen) or above a dielectric ground (i.e., a homogeneous dielectric half-space) with or without losses. The dipole is first taken to be either vertical or horizontal, with the distance from the ground varying according to some properly selected probability distribution. To add more degrees of freedom in the proposed model, the analysis is straightforwardly generalized to an arbitrarily oriented dipole, and the angle defining the orientation of the dipole is also taken to be a random variable. In this respect, the stochastic model introduced and utilized hereinafter aims at assessing the dipole-scatterer interaction using two random variables (but not simultaneously for reasons explained below). Approximate closed-form expressions are obtained for the probability density function (PDF) of the real and imaginary parts of the dipole's input impedance. The resulting formulas are verified via independent Monte-Carlo (MC) simulations exploiting the starting, full-wave expressions regarding the dipole's input impedance. Finally, a few concluding remarks are outlined, and some possible extensions of the present work are discussed.

2. PROBLEM GEOMETRY AND STOCHASTIC MODELING

The problem at hand consists of an elementary electric dipole of length l (much smaller than the operating wavelength λ) and constant current (uniform or equivalent stemming from a triangular distribution), radiating in close proximity to a planar interface extending to infinity in area and in depth, which can be either a perfectly conducting screen or the surface of a homogeneous, either dissipative or lossless, dielectric half-space. The geometry of the problem is shown in Fig. 1 for the cases of vertical, horizontal, and arbitrarily oriented (slanted) dipoles at a height h above the ground. The third case can be treated as a superposition of the first two (see below). Alternatively, the first two cases can be identified as special cases of the third. The purpose of Section 3 below is to provide closed-form expressions for the dipole's input impedance as a function of the distance h between the dipole's center and the planar interface or/and, if necessary, of the angle ψ defining the orientation of the dipole (with respect to the ground plane). When the aforesaid distance or angle is treated as a random variable obeying some known PDF, it is possible to derive approximate analytical expressions for the PDFs of the dipole's input resistance and reactance. Such an approach can aid in assessing the influence of objects lying in the antenna's near-field region upon its input impedance, efficiency, radiating power, and other quantities of theoretical and practical interest.

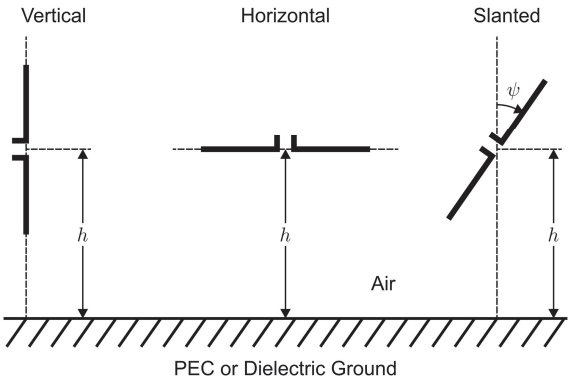

FIGURE 1. Geometry of a vertical, a horizontal, and an arbitrarily oriented infinitesimal electric dipole at a height h above a perfect or imperfect ground plane (infinite scatterer).

With regard to Fig. 1, the dipole can be vertical, horizontal, or arbitrarily oriented, as dictated by the elevation angle ψ. The time dependence $\exp(j\omega t)$ is suppressed throughout the analysis below. The wavenumber in the vacuum (or air) is denoted as $k_0 = 2\pi/\lambda = \omega/c$, where ω denotes the radial frequency, and c stands for the speed of light. The wavenumber in the ground (lower half-space region) is denoted as k, which is related to the respective dielectric permittivity $\varepsilon_r\varepsilon_0$, magnetic permeability μ_0, and electric conductivity σ, as follows

$$k = k_0\sqrt{\varepsilon_r - j\frac{\sigma}{\omega\varepsilon_0}} \tag{1}$$

Both lossy ($\sigma \neq 0$) and lossless ($\sigma = 0$) cases are assumed and examined below.

In Section 3, closed-form expressions are provided for the input impedances of the vertical and horizontal dipoles as a function of h. From these expressions and via superposition, the input impedance of the arbitrarily oriented dipole can be derived as a function of h and ψ. From these and for known PDFs characterizing the variations of h or/and ψ, one can obtain approximate closed-form expressions for the PDFs of the input resistance and reactance separately (or, alternatively, for the respective magnitude and phase). Then, one can further elaborate the probabilistic behavior of the antenna when it operates in the manmade environment, in which the antenna's position or/and orientation change with respect to objects in its close vicinity. Such stochastic models have been used for the assessment of interactions between user and mobile handset (e.g., see [7, 9]). In this paper, the analysis focuses on the change in the antenna's input impedance, which is related to other quantities of theoretical and practical interest.

Albeit perhaps not representative for all interactions between antennas and obstacles/scatterers, the results of this work can be useful as a starting point for more complex cases, as long as realizable antennas can be often subdivided into short sections carrying uniform currents. To this end, one could model more intricate antennas/scatterers with the aid of a (small) number of elementary dipoles (e.g., see [21–27] and other works cited therein) or to attempt to perform a stochastic analysis on the basis of approximate closed-form expressions describing the antenna-scatterer interaction. From these perspectives, the approach of this work can serve as an example (and even as a benchmark case) for generalized approaches or as a basic guide

for performing similar analyses. For example, in the case of an elementary dipole close to a perfectly conducting or dielectric sphere, one can start from the closed-form solution for the scattered EM field around the sphere, then analytically obtain the impedance of the dipole from the tangnetial component of the total electric field at its center (in the form of an intriguing series), and examine the impedance's probabilistic behavior when the antenna-sphere distance varies about a central value.

3. FORMULATION

For the purpose of simplicity, the dipole's input impedance is hereinafter examined after being normalized to the radiation resistance of the infinitesimal dipole in free space $R_0 = \zeta_0(k_0 l)^2/(6\pi)$, where $\zeta_0 \approx 377$ Ohms is the free-space intrinsic impedance [28]. The resulting expressions are conveniently approximated by linear functions (with complex coefficients) with the aim to facilitate the probabilistic analysis. A more advanced, second-order approximation is also discussed and applied.

3.1. Vertical Dipole above a Perfectly Conducting Ground

With regard to the case of a vertical electric dipole above a perfectly conducting ground, the input impedance of the dipole can be easily found using image theory, according to which the exact fields in the air surrounding the dipole can be found via superimposition of the primary fields generated by the dipole in the absence of the ground and the fields generated by an image dipole carrying an equal current flowing towards the same direction. Then, for the input impedance of the primary dipole Z_{in}^v, one can use the well-known relation for a two-element array of identical elements carrying equal currents $Z_{\text{in}}^v = Z_s + Z_m(0, 2h)$ involving the self-impedance Z_s and the mutual impedance $Z_m(0, 2h)$ between parallel electric dipoles separated by zero horizontal distance and by vertical distance equal to $2h$. From the general expression for Z_m provided in Appendix A, the change in the impedance $\Delta Z_{\text{in}}^v = Z_{\text{in}}^v - Z_s$, normalized to R_0, is readily obtained from

$$\frac{\Delta Z_{\text{in}}^v}{R_0} = -\frac{\zeta_0 \exp(-j2k_0 h)}{160\pi}\left(\frac{1}{k_0^2 h^2} - \frac{j}{2k_0^3 h^3}\right) \quad (2)$$

Assuming that $h = h_0 + \Delta h$ with $\Delta h \ll h_0$, one can use the approximations

$$\exp(-j2k_0 h) \approx \exp(-j2k_0 h_0)(1 - j2k_0 \Delta h) \quad (3)$$

$$\frac{1}{h^n} \approx \frac{1}{h_0^n}\left(1 - \frac{n\Delta h}{h_0}\right) \quad n = 2, 3, \ldots \quad (4)$$

Using (3) and (4), and after some algebraic manipulations so as to keep only first-order terms with respect to $\Delta h/h_0$ and neglect the higher-order terms, (2) yields a linear expression of the form $D_v(B_v + C_v \Delta h/h_0)$, where

$$D_v = -\frac{\zeta_0 \exp(-j2k_0 h_0)}{160\pi} \quad (5a)$$

$$B_v = \frac{1}{k_0^2 h_0^2} - \frac{j}{2k_0^3 h_0^3} \quad (5b)$$

$$C_v = -\frac{3}{k_0^2 h_0^2} + j\left(-\frac{2}{k_0 h_0} + \frac{3}{2k_0^3 h_0^3}\right) \quad (5c)$$

3.2. Horizontal Dipole above a Perfectly Conducting Ground

With regard to the case of a horizontal electric dipole above a perfectly conducting ground and similar to the case of the vertical dipole, the exact fields in the air surrounding the dipole can be found via superimposition of the primary fields generated by the dipole in the absence of the ground and the fields generated by an image dipole carrying an equal current flowing towards the opposite direction. Then, for the input impedance of the primary dipole Z_{in}^h, one obtains the expression $Z_{\text{in}}^h = Z_s - Z_m(2h, 0)$ involving Z_s and the mutual impedance $Z_m(2h, 0)$ between parallel electric dipoles separated by a horizontal distance equal to $2h$ and by zero vertical distance. Thus, the change in the impedance $\Delta Z_{\text{in}}^h = Z_{\text{in}}^h - Z_s$, normalized to R_0, is readily obtained from

$$\frac{\Delta Z_{\text{in}}^h}{R_0} = \frac{\zeta_0 \exp(-j2k_0 h)}{160\pi}\left(-\frac{j}{k_0 h} - \frac{1}{2k_0^2 h^2} + \frac{j}{4k_0^3 h^3}\right) \quad (6)$$

Obviously, (6) contains a term analogous to $(k_0 h)^{-1}$ in addition to terms $(k_0 h)^{-2}$ and $(k_0 h)^{-3}$, which is not present in (2). This reveals that the horizontal dipole experiences stronger coupling with the ground over a wider range of h than the vertical dipole (particularly for larger values of $k_0 h$). It is also stressed that the imaginary part is more sensitive than the real part (see Section 4). The latter feature is in line with the large reactance of infinitesimal dipoles, a fact that is rather well known from classic antenna theory.

Assuming that $h = h_0 + \Delta h$ with $\Delta h \ll h_0$ and using the approximations of (3) and (4) while neglecting the higher-order terms, (6) yields a linear expression of the form $D_h(B_h + C_h \Delta h/h_0)$, where

$$D_h = \frac{\zeta_0 \exp(-j2k_0 h_0)}{160\pi} \quad (7a)$$

$$B_h = -\frac{1}{2k_0^2 h_0^2} + j\left(-\frac{1}{k_0 h_0} + \frac{1}{4k_0^3 h_0^3}\right) \quad (7b)$$

$$C_h = -2 + \frac{3}{2k_0^2 h_0^2} + j\left(\frac{2}{k_0 h_0} - \frac{3}{4k_0^3 h_0^3}\right) \quad (7c)$$

3.3. Vertical Dipole above a Dielectric Ground

In the case of a vertical dipole above a lossy/lossless dielectric ground, the change in the input impedance can be found from the approximate closed-form expression [29, Eq. (23.46)], which holds for $|2kh| \gg 1$ and is given by

$$\frac{\Delta Z_{\text{in}}^v}{R_0} \approx \frac{3j \exp(-j2k_0 h)}{8k_0^3 h^3}\frac{k - k_0}{k + k_0}$$

$$\times\left\{1+\frac{4k_0}{k}+j\left[2k_0h+\frac{3}{kh}\left(1-\frac{2k_0}{k}+\frac{3k_0^2}{k^2}\right)\right]\right\} \quad (8)$$

It is particularly stressed that the condition $|2kh| \gg 1$ becomes less important when k is large, which is the case in many real-world scenarios (e.g., for typical soils, concrete walls, human-body tissues).

Again, using the approximations of (3) and (4) while neglecting the higher-order terms, (8) gives $D_v(B_v+C_v\Delta h/h_0)$, where

$$D_v = \frac{3j\exp(-j2k_0h_0)}{8k_0^3h_0^3}\frac{k-k_0}{k+k_0} \quad (9a)$$

$$B_v = 1+\frac{4k_0}{k}+j\left[2k_0h_0+\frac{3}{kh_0}\left(1-\frac{2k_0}{k}+\frac{3k_0^2}{k^2}\right)\right] \quad (9b)$$

$$C_v = -3+4k_0^2h_0^2-\frac{6k_0}{k}\left(1+\frac{2k_0}{k}-\frac{3k_0^2}{k^2}\right) -j\left[6k_0h_0+\frac{8k_0^2h_0}{k}+\frac{12}{kh_0}\left(1-\frac{2k_0}{k}+\frac{3k_0^2}{k^2}\right)\right] \quad (9c)$$

3.4. Horizontal Dipole above a Dielectric Ground

In the case of a horizontal dipole above a lossy/lossless dielectric ground, the change in the input impedance can be found from an approximate closed-form expression [29, Eq. (23.52)], which holds for $|2kh| \gg 1$ and is given by

$$\frac{\Delta Z_{\text{in}}^h}{R_0} \approx \frac{3j\exp(-j2k_0h)}{16k_0^3h^3}\frac{k-k_0}{k+k_0} \times\left\{1-4k_0^2h^2+\frac{2k_0}{k}+j\left[2k_0h+\frac{3}{kh}\left(1-\frac{2k_0}{k}+\frac{3k_0^2}{k^2}\right)\right]\right\} \quad (10)$$

Again, using the approximations of (3) and (4) while neglecting the higher-order terms, (10) gives $D_h(B_h + C_h\Delta h/h_0)$, where

$$D_h=\frac{3j\exp(-j2k_0h_0)}{16k_0^3h_0^3}\frac{k-k_0}{k+k_0} \quad (11a)$$

$$B_h=1+\frac{2k_0}{k}-4k_0^2h_0^2+j\left[2k_0h_0+\frac{3}{kh_0}\left(1-\frac{2k_0}{k}+\frac{3k_0^2}{k^2}\right)\right] \quad (11b)$$

$$C_h=-3+8k_0^2h_0^2+\frac{6k_0^2}{k^2}\left(-2+\frac{3k_0}{k}\right) +j\left[2k_0h_0\left(-3-\frac{2k_0}{k}+4k_0^2h_0^2\right) -\frac{12}{kh_0}\left(1-\frac{2k_0}{k}+\frac{3k_0^2}{k^2}\right)\right] \quad (11c)$$

3.5. Probabilistic Analysis for Vertical and Horizontal Dipoles in Proximity to a Perfectly Conducting or Dielectric Ground

In all the cases examined so far, the normalized impedance change $\Delta Z_{\text{in}}^{v,h}/R_0$ (symbol denoting either $\Delta Z_{\text{in}}^{v}/R_0$ or $\Delta Z_{\text{in}}^{h}/R_0$) is approximated by a linear function of the normalized distance change $\Delta h/h_0$, with the proviso that this last quantity is relatively small ($\Delta h \ll h_0$). Then, one can assume certain PDFs for the auxiliary random variable $\Xi = \Delta h/h_0$ and obtain closed-form expressions for the PDFs governing the real part $\Delta R_{\text{in}}^{v,h}/R_0$ and the imaginary part $\Delta X_{\text{in}}^{v,h}/R_0$ of $\Delta Z_{\text{in}}^{v,h}/R_0 = \Delta R_{\text{in}}^{v,h}/R_0 + j\Delta X_{\text{in}}^{v,h}/R_0$. These expressions can provide valuable insight and condensed information about the behavior and performance of the antenna when it moves with respect to the perfect/imperfect ground. To facilitate the analysis and presentation, the notation $\Pi = \Delta R_{\text{in}}^{v,h}/R_0$ and $\Phi = \Delta X_{in}^{v,h}/R_0$ is used below.

The simplest distribution that one can assume for Ξ is the uniform one with $-\Delta h_{\max} \le \Delta h \le \Delta h_{\max}$, which obeys the PDF $f_\Xi(\xi) = h_0/(2\Delta h_{\max})$, $-\Delta h_{\max}/h_0 \le \xi \le \Delta h_{\max}/h_0$. Then, the ensuing PDFs of Π and Φ are given by the following simple expressions

$$f_\Pi(r) = \frac{1}{|\text{Re}\{D_{v,h}C_{v,h}\}|}\frac{h_0}{2\Delta h_{\max}}, \quad (12a)$$

$$\begin{aligned}&\text{Re}\{D_{v,h}B_{v,h}\}-|\text{Re}\{D_{v,h}C_{v,h}\}|\Delta h_{\max}/h_0\\ &\le r \le \text{Re}\{D_{v,h}B_{v,h}\}\\ &+|\text{Re}\{D_{v,h}C_{v,h}\}|\Delta h_{\max}/h_0\end{aligned}$$

$$f_\Phi(x) = \frac{1}{|\text{Im}\{D_{v,h}C_{v,h}\}|}\frac{h_0}{2\Delta h_{\max}}, \quad (12b)$$

$$\begin{aligned}&\text{Im}\{D_{v,h}B_{v,h}\}-|\text{Im}\{D_{v,h}C_{v,h}\}|\Delta h_{\max}/h_0\\ &\le x \le \text{Im}\{D_{v,h}B_{v,h}\}\\ &+|\text{Im}\{D_{v,h}C_{v,h}\}|\Delta h_{\max}/h_0\end{aligned}$$

where $\text{Re}\{\cdot\}$ and $\text{Im}\{\cdot\}$ denote real and imaginary parts, whereas $|\cdot|$ gives the absolute value of its real argument or the magnitude of its complex argument. The superscript/subscript (v,h) is used to distinguish between the vertical and horizontal cases, which share the same general expressions.

Another choice for the distribution of the random variable Ξ is a truncated Gaussian (or truncated normal) one, which is derived from that of a normally distributed random variable by bounding randomness from below or/and above [30]. The lower and upper bounds can be set so as to realistically describe the inherently non-negative distance $h = h_0 + \Delta h$. Therefore, one can assume $-\Delta h_{\max}/h_0 \le \xi \le \Delta h_{\max}/h_0$ and, consequently, obtain [30]

$$f_\Xi(\xi) = \frac{h_0}{\sqrt{2\pi}\bar{\sigma}}\frac{\exp\left(-\frac{(\xi h_0)^2}{2\bar{\sigma}^2}\right)}{\text{erf}\left(\frac{\Delta h_{\max}}{\sqrt{2}\bar{\sigma}}\right)} \quad (13)$$

where $\text{erf}(\cdot)$ is the well-known error function pertaining to the unit normal distribution, and $\bar{\sigma}^2$ is the variance of the zero-mean parent normal distribution for Δh. For (symmetric) variations

of the zero-mean random variable Ξ obeying (13), the respective variance σ_{Ξ}^2 is given by

$$\sigma_{\Xi}^2 = \frac{\bar{\sigma}^2}{h_0^2}\left[1 - \sqrt{\frac{2}{\pi}}\frac{\Delta h_{\max}}{\bar{\sigma}}\frac{\exp\left(-\frac{(\Delta h_{\max})^2}{2\bar{\sigma}^2}\right)}{\operatorname{erf}\left(\frac{\Delta h_{\max}}{\sqrt{2}\bar{\sigma}}\right)}\right] \tag{14}$$

Then, the PDFs of $\Pi = \Delta R_{\text{in}}^{v,h}/R_0$ and $\Phi = \Delta X_{\text{in}}^{v,h}/R_0$ are given by the following expressions

$$f_{\Pi}(r) = \frac{1}{|\operatorname{Re}\{D_{v,h}C_{v,h}\}|} f_{\Xi}\left(\frac{r - \operatorname{Re}\{D_{v,h}B_{v,h}\}}{\operatorname{Re}\{D_{v,h}C_{v,h}\}}\right), \tag{15a}$$

$$\operatorname{Re}\{D_{v,h}B_{v,h}\} - |\operatorname{Re}\{D_{v,h}C_{v,h}\}|\Delta h_{\max}/h_0 \le r \le \operatorname{Re}\{D_{v,h}B_{v,h}\} + \left|\operatorname{Re}\left\{D_{v,h}C_{v,h}\right\}\right|\Delta h_{\max}/h_0$$

$$f_{\Phi}(x) = \frac{1}{|\operatorname{Im}\{D_{v,h}C_{v,h}\}|} f_{\Xi}\left(\frac{x - \operatorname{Im}\{D_{v,h}B_{v,h}\}}{\operatorname{Im}\{D_{v,h}C_{v,h}\}}\right), \tag{15b}$$

$$\operatorname{Im}\{D_{v,h}B_{v,h}\} - |\operatorname{Im}\{D_{v,h}C_{v,h}\}|\Delta h_{\max}/h_0 \le x \le \operatorname{Im}\{D_{v,h}B_{v,h}\} + |\operatorname{Im}\{D_{v,h}C_{v,h}\}|\Delta h_{\max}/h_0$$

Closed-form expressions for the mean and mean square values associated with (15) are contained in Appendix B.

Other choices for the distribution of the (non-negative) random variable Ξ are possible (e.g., exponential, beta, gamma) and have been tested, but are not presented here due to space limitations.

3.6. Extension to Arbitrarily Oriented Dipoles in Proximity to a Perfectly Conducting or Dielectric Ground

Arbitrarily oriented dipoles above a perfect/imperfect ground can be easily treated with the aid of the formulas derived in Section 3 (Subsections 3.1–3.4). For a dipole with its axis at an arbitrary angle ψ measured from the direction normal to the ground plane of Fig. 1, one can simply divide its current I_0 to a vertical component $I_0\cos\psi$ and to a horizontal component $I_0\sin\psi$. Then, the input impedance of the slanted dipole can be obtained from that of the vertical and horizontal ones, as explained in Appendix A. This procedure leads to the change in the dipole's input impedance due to the presence of the ground scatterer, which is given by

$$\frac{\Delta Z_{\text{in}}}{R_0} = \frac{\Delta Z_{\text{in}}^v}{R_0}(\cos\psi)^2 + \frac{\Delta Z_{\text{in}}^h}{R_0}(\sin\psi)^2 \tag{16}$$

Then, one can utilize the results of Subsections 3.1–3.4 to obtain explicit closed-form expressions for the arbitrarily oriented dipole under investigation. To this end and after some elementary algebraic manipulation, (16) gives

$$\frac{\Delta Z_{\text{in}}}{R_0} = \frac{1}{2}\left(\frac{\Delta Z_{\text{in}}^v}{R_0} + \frac{\Delta Z_{\text{in}}^h}{R_0}\right) + \frac{1}{2}\left(\frac{\Delta Z_{\text{in}}^v}{R_0} - \frac{\Delta Z_{\text{in}}^h}{R_0}\right)\cos(2\psi) \tag{17}$$

Given the form of (17), it is deduced that for a slanted dipole having a fixed ψ and varying h, $\Delta Z_{\text{in}}/R_0$ is given by a linear combination of $\Delta Z_{\text{in}}^v/R_0$ and $\Delta Z_{\text{in}}^h/R_0$, which yields a lengthy function of h that can be treated in a way similar to that followed for the vertical/horizontal dipole cases. The ensuing PDF of $\Delta Z_{\text{in}}/R_0$ is not provided here due to space limitations. If ψ and h vary simultaneously, one has to apply the procedure for obtaining the PDF of a linear combination of two independent random variables when $\Delta h/h_0$ remains small and of a nonlinear one when the small $\Delta h/h_0$ assumption cannot be justified. In both the latter cases, the mathematical manipulation becomes complicated, and the analysis is left for a future paper.

Assuming that the angle ψ varies randomly according to some known PDF $f_{\Psi}(\psi)$ with the height h kept unaltered, one can readily obtain the PDFs of $\Pi = \Delta R_{\text{in}}/R_0$ and $\Phi = \Delta X_{\text{in}}/R_0$. When ψ is uniformly distributed in the range $0 \le \psi \le \pi/2$, $f_{\Psi}(\psi) = 2/\pi$ and the resulting PDFs are given by

$$f_{\Pi}(r) = \frac{2}{\pi\left|\frac{\Delta R_{\text{in}}^v}{R_0} - \frac{\Delta R_{\text{in}}^h}{R_0}\right|}\left\{1 - \left[\frac{r - \frac{1}{2}\left(\frac{\Delta R_{\text{in}}^v}{R_0} + \frac{\Delta R_{\text{in}}^h}{R_0}\right)}{\frac{1}{2}\left(\frac{\Delta R_{\text{in}}^v}{R_0} - \frac{\Delta R_{\text{in}}^h}{R_0}\right)}\right]^2\right\}^{-1/2}, \tag{18a}$$

$$\min\left\{\frac{\Delta R_{\text{in}}^v}{R_0}, \frac{\Delta R_{\text{in}}^h}{R_0}\right\} \le r \le \max\left\{\frac{\Delta R_{\text{in}}^v}{R_0}, \frac{\Delta R_{\text{in}}^h}{R_0}\right\}$$

$$f_{\Phi}(x) = \frac{2}{\pi\left|\frac{\Delta X_{\text{in}}^v}{R_0} - \frac{\Delta X_{\text{in}}^h}{R_0}\right|}\left\{1 - \left[\frac{x - \frac{1}{2}\left(\frac{\Delta X_{\text{in}}^v}{R_0} + \frac{\Delta X_{\text{in}}^h}{R_0}\right)}{\frac{1}{2}\left(\frac{\Delta X_{\text{in}}^v}{R_0} - \frac{\Delta X_{\text{in}}^h}{R_0}\right)}\right]^2\right\}^{-1/2}, \tag{18b}$$

$$\min\left\{\frac{\Delta X_{\text{in}}^v}{R_0}, \frac{\Delta X_{\text{in}}^h}{R_0}\right\} \le x \le \max\left\{\frac{\Delta X_{\text{in}}^v}{R_0}, \frac{\Delta X_{\text{in}}^h}{R_0}\right\}$$

Obviously, these PDFs are nonuniform. Their first and second moments can be readily obtained directly from (17) and are omitted for brevity.

When ψ varies uniformly within a small range about an average value ψ_0, one can write $\psi = \psi_0 + \Delta\psi$ with $-\Delta\psi_{\max} \le \Delta\psi \le \Delta\psi_{\max}$ and use the approximation $\cos[2(\psi_0 + \Delta\psi)] \approx \cos(2\psi_0) - 2\sin(2\psi_0)\Delta\psi$ to obtain

$$\frac{\Delta Z_{\text{in}}}{R_0} \approx \frac{1}{2}\left(\frac{\Delta Z_{\text{in}}^v}{R_0} + \frac{\Delta Z_{\text{in}}^h}{R_0}\right) + \frac{1}{2}\left(\frac{\Delta Z_{\text{in}}^v}{R_0} - \frac{\Delta Z_{\text{in}}^h}{R_0}\right)\cos(2\psi_0) - \left[\left(\frac{\Delta Z_{\text{in}}^v}{R_0} - \frac{\Delta Z_{\text{in}}^h}{R_0}\right)\sin(2\psi_0)\right]\Delta\psi \tag{19}$$

which readily leads to the (approximately uniform) PDFs that follow

$$f_{\Pi}(r) = \frac{1}{2\left|\left(\frac{\Delta R_{\text{in}}^v}{R_0} - \frac{\Delta R_{\text{in}}^h}{R_0}\right)\sin(2\psi_0)\right|\Delta\psi_{\max}}, \tag{20a}$$

$$\frac{1}{2}\left(\frac{\Delta R_{\text{in}}^v}{R_0} + \frac{\Delta R_{\text{in}}^h}{R_0}\right) + \frac{1}{2}\left(\frac{\Delta R_{\text{in}}^v}{R_0} - \frac{\Delta R_{\text{in}}^h}{R_0}\right)\cos(2\psi_0) - \left|\left(\frac{\Delta R_{\text{in}}^v}{R_0} - \frac{\Delta R_{\text{in}}^h}{R_0}\right)\sin(2\psi_0)\right|\Delta\psi_{\max} \le r \le \frac{1}{2}\left(\frac{\Delta R_{\text{in}}^v}{R_0} + \frac{\Delta R_{\text{in}}^h}{R_0}\right) + \frac{1}{2}\left(\frac{\Delta R_{\text{in}}^v}{R_0} - \frac{\Delta R_{\text{in}}^h}{R_0}\right)\cos(2\psi_0)$$

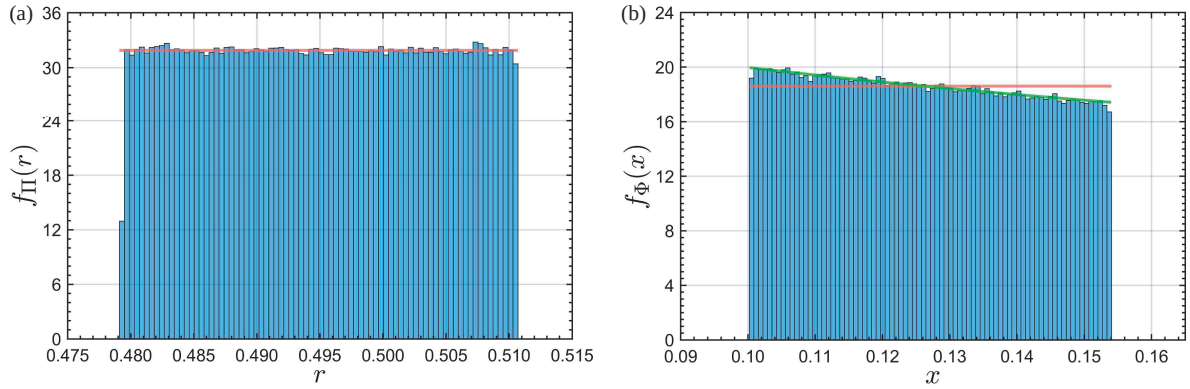

FIGURE 2. (a) The PDF of $\Pi = \Delta R_{\text{in}}^v/R_0$ as obtained from (12a) along with (5); (b) The PDF of $\Phi = \Delta X_{\text{in}}^v/R_0$ as obtained from (12b) along with (5). The histograms were produced by an independent MC code exploiting (2). The results are for $f = 1$ GHz, a perfectly conducting ground, and h uniformly distributed with $h_0 = \lambda/5$ and $\Delta h_{\max} = h_0/50$. Fig. 2(b) also illustrates the PDF of $\Phi = \Delta X_{\text{in}}^v/R_0$ as obtained from the second-order approximation of Appendix C (green line).

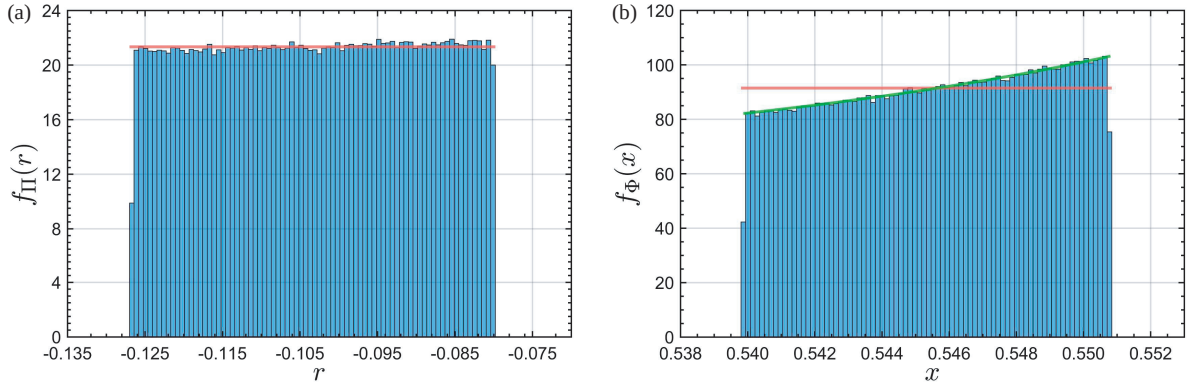

FIGURE 3. (a) The PDF of $\Pi = \Delta R_{\text{in}}^h/R_0$ as obtained from (12a) along with (7); (b) The PDF of $\Phi = \Delta X_{\text{in}}^h/R_0$ as obtained from (12b) along with (7). The histograms were produced by an independent MC code exploiting (6). The other parameters are as in Fig. 2. Fig. 3(b) also illustrates the PDF of $\Phi = \Delta X_{\text{in}}^h/R_0$ as obtained from the second-order approximation of Appendix C (green line).

$$
\begin{aligned}
&+\left|\left(\frac{\Delta R_{\text{in}}^v}{R_0}-\frac{\Delta R_{\text{in}}^h}{R_0}\right)\sin(2\psi_0)\right|\Delta\psi_{\max}\\
f_\Phi(x)=&\frac{1}{2\left|\left(\frac{\Delta X_{\text{in}}^v}{R_0}-\frac{\Delta X_{\text{in}}^h}{R_0}\right)\sin(2\psi_0)\right|\Delta\psi_{\max}},\\
&\frac{1}{2}\left(\frac{\Delta X_{\text{in}}^v}{R_0}+\frac{\Delta X_{\text{in}}^h}{R_0}\right)+\frac{1}{2}\left(\frac{\Delta X_{\text{in}}^v}{R_0}-\frac{\Delta X_{\text{in}}^h}{R_0}\right)\cos(2\psi_0)\\
&-\left|\left(\frac{\Delta X_{\text{in}}^v}{R_0}-\frac{\Delta X_{\text{in}}^h}{R_0}\right)\sin(2\psi_0)\right|\Delta\psi_{\max}\le x\\
\le&\frac{1}{2}\left(\frac{\Delta X_{\text{in}}^v}{R_0}+\frac{\Delta X_{\text{in}}^h}{R_0}\right)+\frac{1}{2}\left(\frac{\Delta X_{\text{in}}^v}{R_0}-\frac{\Delta X_{\text{in}}^h}{R_0}\right)\cos(2\psi_0)\\
&+\left|\left(\frac{\Delta X_{\text{in}}^v}{R_0}-\frac{\Delta X_{\text{in}}^h}{R_0}\right)\sin(2\psi_0)\right|\Delta\psi_{\max}
\end{aligned}
\tag{20b}
$$

4. RESULTS

This Section contains numerical results for the cases discussed in Section 3. These results were obtained from self-developed computer codes based on the formulation of this work.

First, results are presented for vertical and horizontal dipoles located at an average height equal to $h_0{=}\lambda/5$ above a perfectly conducting ground, where λ is the wavelength corresponding to $f{=}\,1$ GHz. The distance h is assumed to vary uniformly about h_0, with maximum deviation $\Delta h_{\max}{=}h_0/50$. The PDFs of the normalized resistance and reactance changes, as computed from (12) with the aid of (5) (for the vertical dipole) or (7) (for the horizontal dipole), are shown in Fig. 2 for the vertical dipole and in Fig. 3 for the horizontal dipole, along with independent histograms obtained from an MC code exploiting the rigorous full expressions of (2) and (6), respectively. Obviously, the results from the approximate closed-form expressions agree quite well with the MC ones, especially the real parts. The behavior of the imaginary parts seems to deviate more notably from uniformity in Fig. 3 [compare Fig. 3(b) with Fig. 2(b)], as one could expect from the fact that the horizontal dipole is more strongly affected by the presence of the ground. To mitigate the discrepancies in the imaginary parts, a more accurate model can be obtained by keeping the second-order term $(\Delta h/h_0)^2$ in the analysis of Section 3. The resulting, rather lengthy, expressions are provided in Appendix C and the improved numerical results corresponding to the cases considered so far in this Section are

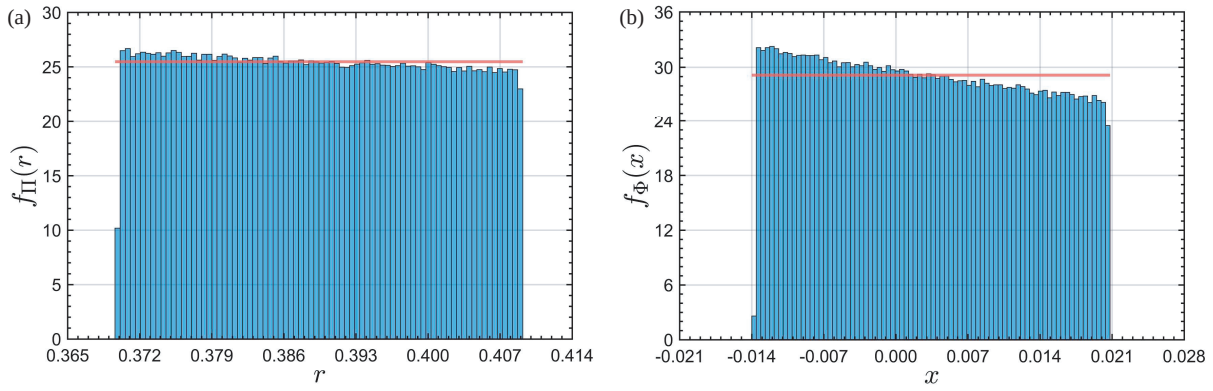

FIGURE 4. Like Fig. 2 but for an imperfectly conducting ground with $\varepsilon_r = 13$ and $\sigma = 0.01$ S/m at $f = 1$ GHz, the PDFs were obtained from (12) along with (9). The histograms were produced by an independent MC code exploiting (8).

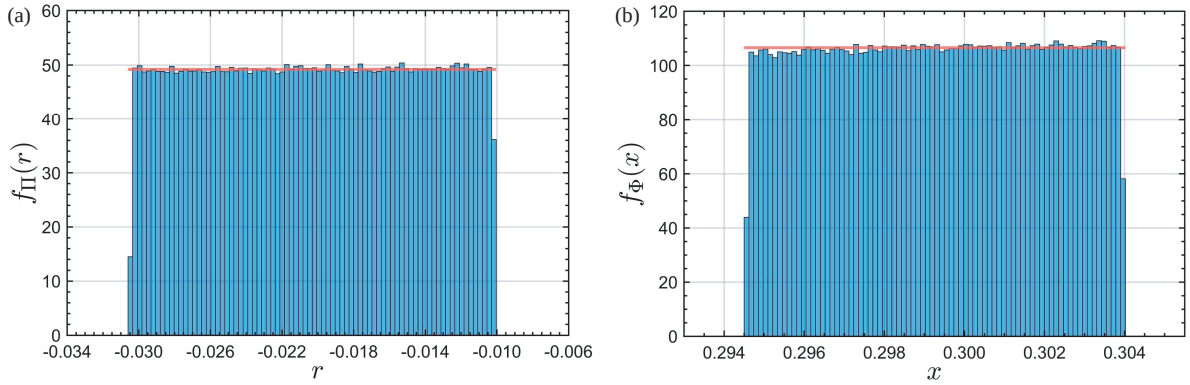

FIGURE 5. Like Fig. 3 but for an imperfectly conducting ground with $\varepsilon_r = 13$ and $\sigma = 0.01$ S/m at $f = 1$ GHz, the PDFs were obtained from (12) along with (11). The histograms were produced by an independent MC code exploiting (10).

depicted in Fig. 2(b) and Fig. 3(b) (green lines), alongside the rough results of the first-order approximation and the MC ones. The improvement in the accuracy of the results is obvious and should be expected for $\Delta h_{\max}$ at least up to $\Delta h_{\max}{=}h_0/20$.

A similar behavior is revealed in Figs. 4 and 5 for the cases of the vertical and horizontal dipoles above a dielectric ground having $\varepsilon_r{=}\ 13$ and $\sigma{=}\ 0.01$ S/m at the selected frequency $f{=}\ 1$ GHz (corresponding to a dry soil [31]). The results shown in Figs. 4 and 5 were computed using (8)–(12) and are representative of what one should expect over a wide range of frequencies and soil parameters. It is again evident that the approximate formulas (12) for the PDFs work very well, at least when $\Delta h_{\max}$ is kept sufficiently small. Again, as already deduced from Figs. 2 and 3, the agreement is less satisfactory for the imaginary parts than the real parts and for the horizontal dipole than the vertical dipole, but the discrepancies are less profound than those of Figs. 2 and 3. As $\Delta h_{\max}$ is increased with respect to h_0, the first-order approximations that yielded (5), (7), (9), and (11) become less accurate, and the resulting PDFs begin to deviate more notably from the exact ones and from the respective MC histograms. On the other hand, the computation of the latter is much more demanding, in terms of execution time and memory than that required by the approximate closed-form PDFs. For the MC results shown in this work for the purpose of comparison, 10^6 runs were found to generate trustworthy histograms. No effort has been put to optimize MC simulations and minimize the number of runs.

Next, numerical results are presented in Figs. 6 and 7 for the vertical and horizontal dipoles above the aforesaid imperfect ground when h varies according to the truncated Gaussian distribution with $\Delta h_{\max}{=}h_0/20$ and $\bar{\sigma}\ =\ h_0/50$. Again, the results of these approximate formulas are verified by the independent MC histograms obtained using (8) and (10). As $\bar{\sigma}$ gets larger, the PDFs of $\Delta R_{\text{in}}^{v,h}/R_0$ and $\Delta X_{\text{in}}^{v,h}/R_0$ tend to become nearly uniform, as long as the truncated Gaussian distribution of (13) tends to become mostly flat. This behavior should be expected for other distributions with large dispersion and has indeed been observed in the results of several numerical tests, which are not shown here due to space limitations.

Numerical results for slanted dipoles are also provided. First, for a dipole above a perfectly conducting ground at $h_0 = \lambda/5$ and for ψ varying in the range $0 \leq \psi \leq \pi/2$, the PDFs resulting from (18) are shown in Fig. 8, which also illustrates their agreement to the respective MC histograms obtained from (16) [or its equivalent (17)], along with (2) and (6). Notably, the PDFs of $\Delta R_{\text{in}}/R_0$ and $\Delta X_{\text{in}}/R_0$ are not uniform but curved upwards and exhibit sharp peaks at the ends. Numerous tests have revealed that these PDFs tend to become almost flat when ψ varies uniformly within a small range about any arbitrarily selected ψ_0. The results ensuing from (20), (8), and (10) for ψ

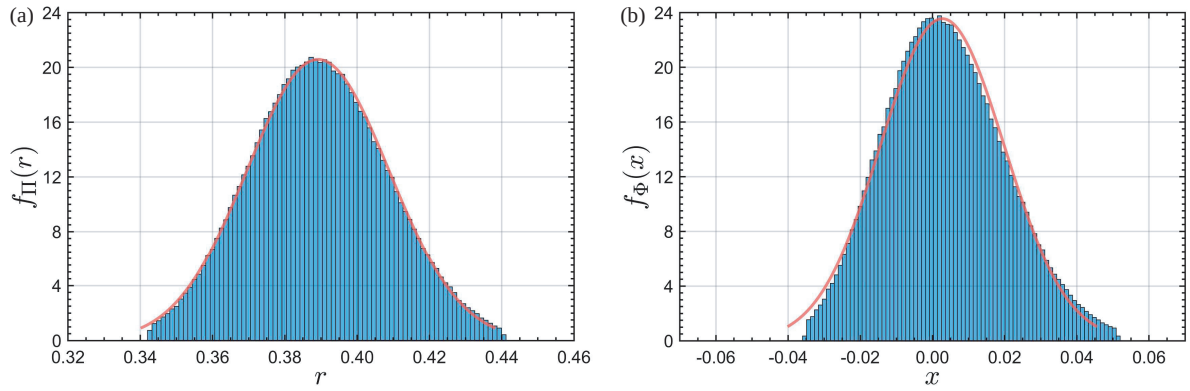

FIGURE 6. Like Fig. 4 but for h varying according to the truncated Gaussian distribution with $\Delta h_{\max}{=}h_0/20$ and $\bar{\sigma} = h_0/50$, the PDFs were obtained from (15) and (13), whereas the histograms were produced by an independent MC code exploiting (8).

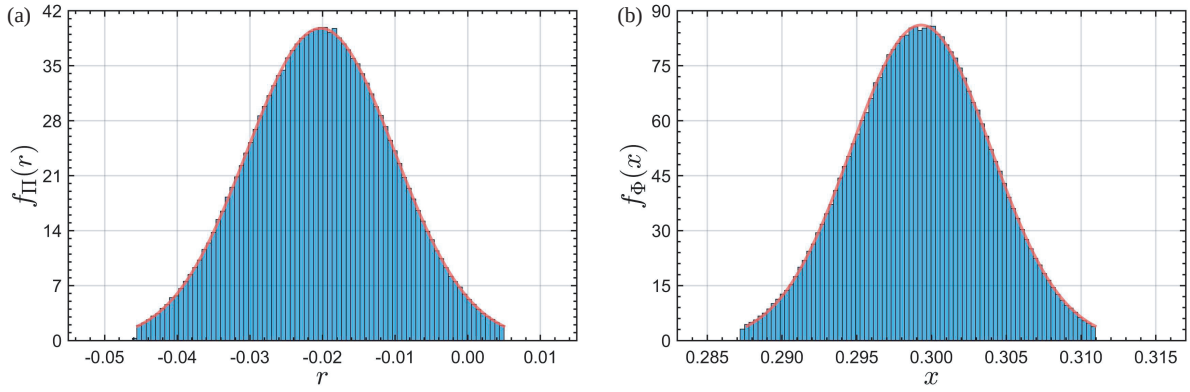

FIGURE 7. Like Fig. 5 but for h varying according to the truncated Gaussian distribution with $\Delta h_{\max}{=}h_0/20$ and $\bar{\sigma} = h_0/50$, the PDFs were obtained from (15) and (13), whereas the histograms were produced by an independent MC code exploiting (10).

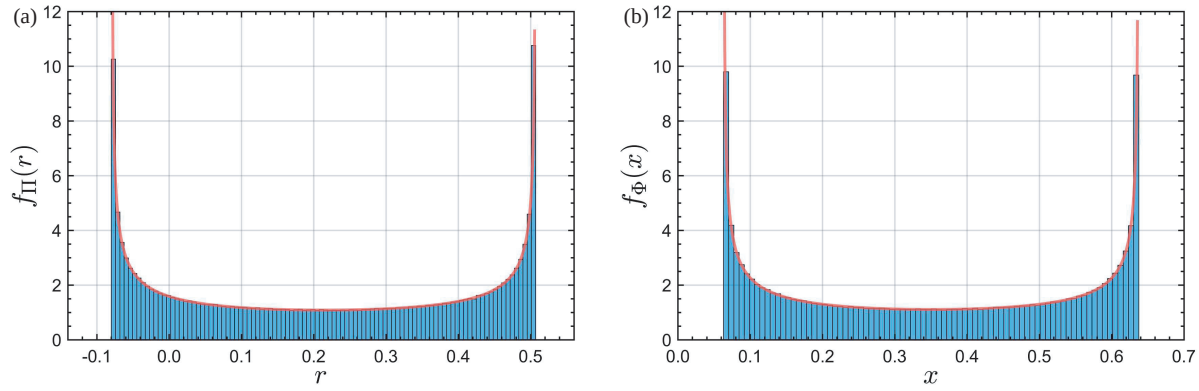

FIGURE 8. (a) The PDF of $\Pi = \Delta R_{\text{in}}/R_0$ as obtained from (18a), (5), and (7); (b) The PDF of $\Phi = \Delta X_{\text{in}}/R_0$ as obtained from (18b), (5), and (7). The histograms were produced by an independent MC code exploiting (16) [or (17)] along with (2) and (6). The results are for $f = 1\,\text{GHz}$, a perfectly conducting ground, $h_0 = \lambda/5$, and ψ varying in the range $0 \leq \psi \leq \pi/2$.

varying uniformly about $\psi_0 = \pi/5$ with $\Delta\psi_{\max} = \pi/50$ are shown in Fig. 9. This time, the dipole was taken to be placed at $h_0 = \lambda/5$ above a dielectric ground plane having the same parameters as before. It was again verified that this flatness also occurs for the case of the perfect ground and for arbitrary combinations of h_0 and ψ_0.

5. CONCLUDING REMARKS AND DISCUSSION ON POSSIBLE EXTENSIONS

Antennas are most often studied in free space, isolated from real-world obstacles/scatterers, mainly in order to facilitate the analysis and obtain radiated fields and pertinent parameters of interest, either analytically or numerically, for as low computa-

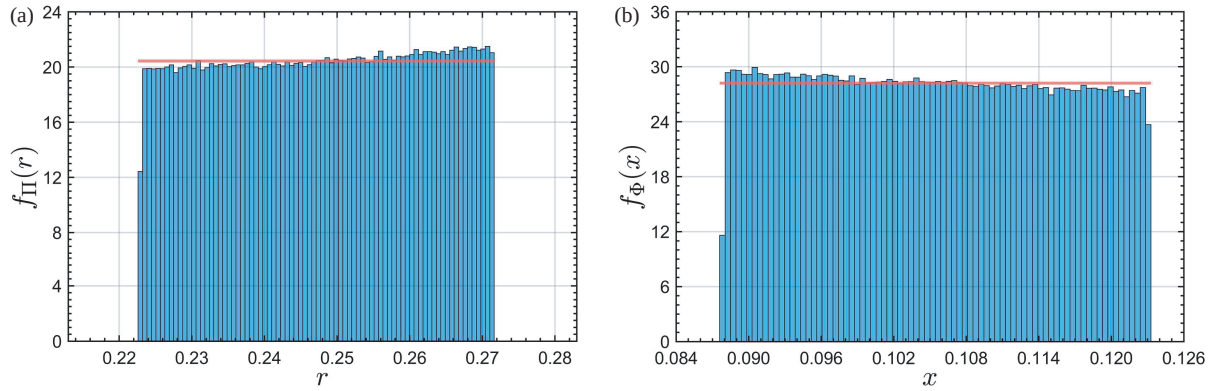

FIGURE 9. (a) The PDF of $\Pi = \Delta R_{\text{in}}/R_0$ as obtained from (20a), (8), and (10); (b) The PDF of $\Phi = \Delta X_{\text{in}}/R_0$ as obtained from (20b), (8), and (10). The histograms were produced by an independent MC code exploiting (8) and (10). The results are for $f = 1$ GHz, an imperfectly conducting ground with $\varepsilon_r = 13$ and $\sigma = 0.01$ S/m at $f = 1$ GHz, and for ψ varying uniformly about $\psi_0 = \pi/5$ with $\Delta\psi_{\text{max}} = \pi/50$.

tional cost as possible. Nevertheless, real antennas usually operate in close proximity to obstacles/scatterers of various types (from masts and support structures to user heads/arms/bodies, walls, plants, as well as all kinds of indoor objects). Therefore, the conclusions drawn from the study of an antenna subject to the underlying assumptions and notions for the existence (or non-existence) of other objects may be incomplete and misleading, and can undermine the performance of the actual wireless system exploiting the antenna.

To overcome the aforesaid deficiencies and given the fact that antenna-obstacle/scatterer arrangements are rarely mutually motionless (especially in the contemporary manmade environment), stochastic approaches that somehow incorporate spatial/temporal variations seem more promising and are often adopted by researchers instead of deterministic ones. This work aims at investigating how an elementary dipole is affected by the presence of a ground plane, which is the simplest type of obstacle/scatterer, when the distance/angle between them varies in accordance with simple and reasonable probability distributions. The ensuing closed-form PDFs for the input resistance/reactance provide a basis for delving deeper into the probabilistic behavior of the antenna and can be useful when studying more intricate antennas or antennas that are modeled with the aid of elementary dipoles. To facilitate the analysis of this paper, only simple scenarios involving one random variable obeying reasonable and tractable distributions were presented. The results discussed regarded the PDFs of the resistance and reactance separately, which revealed their dependence upon the specificities of the height and angle distributions.

Scenarios involving canonical obstacle/scatterer geometries (e.g., spherical or cylindrical ones) may be tractable using available closed-form solutions (as starting point) along with some stochastic strategy for incorporating spatial/temporal randomness. However, as long as the analytical derivation of closed-form expressions for PDFs or other related functions (e.g., cumulative probability functions, characteristic functions) and comprehensive quantities (e.g., moments) is (almost) impossible for complex real-world scenarios, non-analytical methods could be utilized to assess the performance of antennas close to non-canonical objects.

Future extensions of the present work could focus on antennas in the presence of spheres or cylinders, or even close to human head/body phantoms, provided that exact or approximate closed-form expressions for the input impedance (or other quantities of interest) exist (or can be deduced). The approach of this work can be viewed as another step towards a generalized strategy for assessing composite antennas and arrays in the contemporary manmade environment.

ACKNOWLEDGMENT

The authors would like to thank Prof. C. Vazouras of the Hellenic Naval Academy for useful discussions and suggestions regarding the soil parameters.

APPENDIX A.

This Appendix provides results from the method of induced electromotive force (IEMF) [32]. The self-impedance of a straight-wire antenna is given by

$$Z_s = -\frac{1}{I_0^2}\int_{-\frac{l}{2}}^{\frac{l}{2}} I(w)\,\vec{E}_l(w)\cdot d\vec{w} \tag{A1}$$

where l is the length of the antenna, I_0 the driving-point current, $I(w)$ the current distribution along the wire, $E_l(w)$ the longitudinal component of the produced electric field along the wire, and w the integration variable.

With regard to the mutual impedance between two identical elementary electric dipoles, which are parallel and staggered so as to have horizontal separation distance d and vertical separation distance s, one can start from a similar expression for the mutual impedance, which involves the product of the current along one of the two dipoles with the corresponding electric field produced by the other dipole, as follows

$$Z_m = -\frac{1}{I_1 I_2}\int_{-\frac{l}{2}}^{\frac{l}{2}} I_1(w)\,\vec{E}_{2,1}(w)\cdot d\vec{w}$$

$$= -\frac{1}{I_1 I_2}\int_{-\frac{l}{2}}^{\frac{l}{2}} I_2(w)\,\vec{E}_{1,2}(w)\cdot d\vec{w} \qquad \text{(A2)}$$

This last expression is an outcome of the reciprocity theorem and can be readily generalized to arbitrary antennas.

For dipoles carrying constant currents and having length l shorter than the operating wavelength λ, the mutual impedance $Z_m(d,s)$ can be readily obtained from the longitudinal near-field component produced from any of the two dipoles at the center of the other, which yields

$$\begin{aligned} Z_m(d,s) &= -\frac{\zeta_0 l^2}{4\pi} e^{-jk_0\sqrt{d^2+s^2}} \\ &\times\left\{\frac{2s^2}{d^2+s^2}\left[\frac{1}{d^2+s^2}-j\frac{1}{k_0\left(d^2+s^2\right)^{3/2}}\right]\right. \\ &-\frac{d^2}{d^2+s^2}\left[\frac{1}{d^2+s^2}+j\left(\frac{k_0}{\left(d^2+s^2\right)^{1/2}}\right.\right. \\ &\left.\left.\left.-\frac{1}{k_0\left(d^2+s^2\right)^{3/2}}\right)\right]\right\} \end{aligned} \qquad \text{(A3)}$$

For a wire antenna at an arbitrary angle as in Fig. 1, the electric-field vector can be expressed in terms of the respective vertical ($E_v\cos\psi$) and horizontal ($E_h\sin\psi$) components. Then, for $l \ll \lambda$ and uniform current $I(w) = I_0$, the integral in (A1) immediately yields

$$Z_s = Z_s^v\left(\cos\psi\right)^2 + Z_s^h\left(\sin\psi\right)^2 \qquad \text{(A4)}$$

Finally, (A4) readily gives (16).

APPENDIX B.

This Appendix provides the mean square values and standard deviations associated with (15). The mean values are simply $E\{\Delta R_{\text{in}}^{v,h}/R_0\} = \text{Re}\{D_{v,h}B_{v,h}\}$ and $E\{\Delta X_{\text{in}}^{v,h}/R_0\} = \text{Im}\{D_{v,h}B_{v,h}\}$. The mean square values can be found via some straightforward algebra

$$\begin{aligned} E\left\{\left(\frac{\Delta R_{\text{in}}^{v,h}}{R_0}\right)^2\right\} &= \left(\text{Re}\{D_{v,h}B_{v,h}\}\right)^2 + \bar{\sigma}^2\frac{\left(\text{Re}\{D_{v,h}C_{v,h}\}\right)^2}{h_0^2} \\ &\times\left[1-\sqrt{\frac{2}{\pi}}\frac{\Delta h_{\max}\exp\left(-\frac{(\Delta h_{\max})^2}{2\bar{\sigma}^2}\right)}{\bar{\sigma}\,\text{erf}\left(\frac{\Delta h_{\max}}{\sqrt{2}\bar{\sigma}}\right)}\right] \end{aligned} \qquad \text{(B1)}$$

$$\begin{aligned} E\left\{\left(\frac{\Delta X_{\text{in}}^{v,h}}{R_0}\right)^2\right\} &= \left(\text{Im}\{D_{v,h}B_{v,h}\}\right)^2 + \bar{\sigma}^2\frac{\left(\text{Im}\{D_{v,h}C_{v,h}\}\right)^2}{h_0^2} \\ &\times\left[1-\sqrt{\frac{2}{\pi}}\frac{\Delta h_{\max}\exp\left(-\frac{(\Delta h_{\max})^2}{2\bar{\sigma}^2}\right)}{\bar{\sigma}\,\text{erf}\left(\frac{\Delta h_{\max}}{\sqrt{2}\bar{\sigma}}\right)}\right] \end{aligned} \qquad \text{(B2)}$$

The second terms in the summations in (B1) and (B2) provide the respective variances.

APPENDIX C.

This Appendix contains the expressions for the PDFs of Π and Φ ensuing from a procedure similar to that followed in Section 3 when the second-order term is retained. Due to space limitations, only important steps are highlighted below, without presenting the algebraic manipulations.

For the case of the vertical dipole above a perfectly electrically conducting (PEC) ground, the second-order approximation of (2) yields an expression of the form $D_v[B_v + C_v\Delta h/h_0 + E_v(\Delta h/h_0)^2]$, where

$$E_v = -2 + \frac{6}{k_0^2 h_0^2} + j\left(\frac{5}{k_0 h_0} - \frac{3}{k_0^3 h_0^3}\right) \qquad \text{(C1)}$$

Similarly, for the case of the horizontal dipole above a PEC ground, the second-order approximation of (6) yields $D_h[B_h + C_h\Delta h/h_0 + E_h(\Delta h/h_0)^2]$, where

$$E_h = 3 - \frac{3}{k_0^2 h_0^2} + j\left(2k_0 h_0 - \frac{7}{2k_0 h_0} + \frac{3}{2k_0^3 h_0^3}\right) \qquad \text{(C2)}$$

In both cases, for $\Delta h/h_0$ varying uniformly as in Section 3, one can derive the PDFs for both Π and Φ at once. For the latter case, which is more sensitive and prone to approximation errors, one obtains

$$\begin{aligned} f_\Phi(x) &= \frac{h_0}{2\Delta h_{\max}}\left[\left(\text{Im}\{D_{v,h}C_{v,h}\}\right)^2 - 4\text{Im}\{D_{v,h}E_{v,h}\}\right. \\ &\left.\left(\text{Im}\{D_{v,h}B_{v,h}\} - x\right)\right]^{-1/2} \end{aligned} \qquad \text{(C3)}$$

$$\begin{aligned} &\text{Im}\{D_{v,h}B_{v,h}\} - \left|\text{Im}\{D_{v,h}C_{v,h}\}\right|\frac{\Delta h_{\max}}{h_0} \\ &+\text{Im}\{D_{v,h}E_{v,h}\}\left(\frac{\Delta h_{\max}}{h_0}\right)^2 \\ &\le x \le \text{Im}\{D_{v,h}B_{v,h}\} + \left|\text{Im}\{D_{v,h}C_{v,h}\}\right|\frac{\Delta h_{\max}}{h_0} \\ &+\text{Im}\{D_{v,h}E_{v,h}\}\left(\frac{\Delta h_{\max}}{h_0}\right)^2 \end{aligned}$$

REFERENCES

[1] Jensen, M. A. and Y. Rahmat-Samii, "EM interaction of handset antennas and a human in personal communications," *Proceedings of the IEEE*, Vol. 83, No. 1, 7–17, Jan. 1995.

[2] Krogerus, J., J. Toivanen, C. Icheln, and P. Vainikainen, "Effect of the human body on total radiated power and the 3-D radiation pattern of mobile handsets," *IEEE Transactions on Instrumentation and Measurement*, Vol. 56, No. 6, 2375–2385, Dec. 2007.

[3] Holopainen, J., O. Kivekäs, J. Ilvonen, R. Valkonen, C. Icheln, and P. Vainikainen, "Effect of the user's hands on the operation of lower UHF-band mobile terminal antennas: Focus on digital television receiver," *IEEE Transactions on Electromagnetic Compatibility*, Vol. 53, No. 3, 831–841, Aug. 2011.

[4] Boyle, K. R., Y. Yuan, and L. P. Ligthart, "Analysis of mobile phone antenna impedance variations with user proximity," *IEEE Transactions on Antennas and Propagation*, Vol. 55, No. 2, 364–372, Feb. 2007.

[5] Rahman, N. B. A., A. A. Al-Hadi, and S. N. Azemi, "Impedance analysis of mobile phone antenna in the presence of user's hand," in *2017 International Conference on Emerging Electronic Solutions for IoT*, Vol. 140, 01031, Dec. 2017.

[6] Houdzoumis, V. A., "Vertical electric dipole radiation over a sphere: Character of the waves that propagate through the sphere," *Journal of Applied Physics*, Vol. 86, No. 7, 3939–3942, 1999.

[7] Vellis, F. E. and C. N. Capsalis, "A model for the statistical characterisation of fast fading in the presence of a user," *Wireless Personal Communications*, Vol. 15, 207–219, 2000.

[8] Warne, L. K., K. S. H. Lee, H. G. Hudson, W. A. Johnson, R. E. Jorgenson, and S. L. Stronach, "Statistical properties of linear antenna impedance in an electrically large cavity," *IEEE Transactions on Antennas and Propagation*, Vol. 51, No. 5, 978–992, May 2003.

[9] Nadarajah, S. and S. Kotz, "A class of VeCa distributions for the statistical modeling of fast fading," *Wireless Personal Communications*, Vol. 42, 13–21, 2007.

[10] Glazunov, A. A., A. F. Molisch, and F. Tufvesson, "Mean effective gain of antennas in a wireless channel," *IET Microwaves, Antennas & Propagation*, Vol. 3, No. 2, 214–227, 2009.

[11] Pelosi, M., O. Franek, M. B. Knudsen, G. F. Pedersen, and J. B. Andersen, "Antenna proximity effects for talk and data modes in mobile phones," *IEEE Antennas and Propagation Magazine*, Vol. 52, No. 3, 15–27, Jun. 2010.

[12] Lin, Y. and W. Yu, "Downlink spectral efficiency of distributed antenna systems under a stochastic model," *IEEE Transactions on Wireless Communications*, Vol. 13, No. 12, 6891–6902, Dec. 2014.

[13] Rossi, M., G.-J. Stockman, H. Rogier, and D. V. Ginste, "Stochastic analysis of the efficiency of a wireless power transfer system subject to antenna variability and position uncertainties," *Sensors*, Vol. 16, No. 7, 1100, 2016.

[14] Syrytsin, I., S. Zhang, G. F. Pedersen, K. Zhao, T. Bolin, and Z. Ying, "Statistical investigation of the user effects on mobile terminal antennas for 5G applications," *IEEE Transactions on Antennas and Propagation*, Vol. 65, No. 12, 6596–6605, Dec. 2017.

[15] Carro, P. L., J. d. Mingo, P. García-Dúcar, and A. Valdovinos, "Statistical antenna proximity effect modeling with uncertainty impedance ellipses," *International Journal of Antennas and Propagation*, Vol. 2017, No. 1, 7192491, 2017.

[16] Ufiteyezu, E. and Y. Li, "Stochastic and deterministic framework for modeling the effect of antennas location error on DOA estimation," *IEEE Access*, Vol. 8, 4785–4798, 2019.

[17] Lee, S. and H.-J. Song, "Accurate statistical model of radiation patterns in analog beamforming including random error, quantization error, and mutual coupling," *IEEE Transactions on Antennas and Propagation*, Vol. 69, No. 7, 3886–3898, Jul. 2021.

[18] Sipus, Z., A. Šušnjara, A. K. Skrivervik, D. Poljak, and M. Bosiljevac, "Influence of uncertainty of body permittivity on achievable radiation efficiency of implantable antennas — Stochastic analysis," *IEEE Transactions on Antennas and Propagation*, Vol. 69, No. 10, 6894–6905, Oct. 2021.

[19] Galić, M., A. Šušnjara, and D. Poljak, "Stochastic-deterministic assessment of electric field radiated by base station antenna above a two-layered ground," *Mathematical Problems in Engineering*, Vol. 2022, No. 1, 1833748, 2022.

[20] Kanters, N. and A. A. Glazunov, "Stochastic array antenna figures-of-merit for quality-of-service-enhanced massive MIMO," *Electronics Letters*, Vol. 60, No. 2, e13064, 2024.

[21] Hansen, T. B., "Complex-point dipole formulation of probe-corrected cylindrical and spherical near-field scanning of electromagnetic fields," *IEEE Transactions on Antennas and Propagation*, Vol. 57, No. 3, 728–741, Mar. 2009.

[22] Diamantis, S. G., A. P. Orfanidis, G. A. Kyriacou, and J. N. Sahalos, "Hybrid mode matching and auxiliary sources technique for horn antenna analysis," *Microwave and Optical Technology Letters*, Vol. 49, No. 3, 734–739, 2007.

[23] Bae, E., H. Zhang, and E. D. Hirleman, "Application of the discrete dipole approximation for dipoles embedded in film," *Journal of the Optical Society of America A*, Vol. 25, No. 7, 1728–1736, 2008.

[24] Wu, X. H., A. A. Kishk, and A. W. Glisson, "Modeling of wideband antennas by frequency-dependent hertzian dipoles," *IEEE Transactions on Antennas and Propagation*, Vol. 56, No. 8, 2481–2489, Aug. 2008.

[25] Petoev, I. M., V. A. Tabatadze, D. G. Kakulia, and R. S. Zaridze, "Method of auxiliary sources applied to thin plates and open surfaces," *Journal of Communications Technology and Electronics*, Vol. 60, 311–320, 2015.

[26] Kwak, K., T.-i. Bae, K. Hong, H. Kim, and J. Kim, "Accuracy investigation of equivalent dipole arrays for near-field estimation in presence of shielding or dielectric structures," *Microwave and Optical Technology Letters*, Vol. 62, No. 4, 1724–1732, 2020.

[27] Jeladze, V. B., T. R. Nozadze, V. A. Tabatadze, I. A. Petoev-Darsavelidze, M. M. Prishvin, and R. S. Zaridze, "Electromagnetic exposure study on a human located inside the car using the method of auxiliary sources," *Journal of Communications Technology and Electronics*, Vol. 65, 457–464, 2020.

[28] Collin, R. E., "Radiation from simple sources," *Antenna Theory*, Vol. 1, 40, 1969.

[29] Wait, J. R., "Characteristics of antennas over lossy earth," *Antenna Theory*, Vol. 2, 329–435, 1969.

[30] Burkardt, J., "The truncated normal distribution," *Department of Scientific Computing, Florida State University*, Vol. 1, No. 35, 58, Oct. 2014.

[31] ITU, "Recommendation ITU-R P.527-6 (Electrical Characteristics of the Surface of the Earth)," 2021.

[32] Balanis, C. A., *Antenna Theory: Analysis and Design*, John Wiley & Sons, 2016.